AJChE 2002, Vol. 2, No. 1, 87-96

Measuring and Modeling the Performance of Rigid Ceramic Filters

*T. G. Chuah, M
Department of Chemical and Environmental Engineering, Faculty of Engineering, Universiti Putra Malaysia, Serdang, UPM, Selangor D.E., Malaysia.
J. P. .K Seville
School of Chemical Engineering, The University of Birmingham, Edgbaston, Birmingham B15 2TT, U.K.

Rigid ceramic filters have been proven to be highly efficient gas filtration devices. However, they must be cleaned periodically for maximum efficiency. This is done by applying a pulsed reverse flow. The cleaning mechanism by which the deposited dirt is removed from the filter surface is still not fully understood. Experiments were carried out to measure pressure drop along the axis of two different candle geometry, cylindrical and tapered. For the cylindrical filter, the reverse pulse pressure was not uniformly distributed along the element. Generally, the pressure difference across the wall of the element is highest at the close end, and lowest, sometimes close to zero, at the open end. Pressure drop across the tapered filter was more uniform compared to that of the cylindrical filter. Hence, it should demonstrate better filter dirt removal. The authors have written a computer program that models the flow of the reverse pulse from the cleaning bar nozzle to the dirty side of the filter. It uses the iterative calculation mode and allows variables such as reverse pulse pressure and filter geometry to be changed. The calculations demonstrate fair agreement with the experimental results.

Keywords: gas filtration, ceramic filter, pulse cleaning, modelling, flow dynamics, tapered-filter

INTRODUCTION

Rigid ceramic filters offer the most promising technology for the removal of particulate from process gases at high temperature. Ceramic filters are normally used in the form of "candles"- cylindrical tubes with permeable walls. Two generic types are available, with those granular and fibrous structures.

Effective cleaning of the filter element is as important as the filtration process, thus it is important to study gas flow dynamics in the reverse flow mode in order to achieve better filter cleaning. Several studies have been carried out on pulse gas cleaning (Berbner and Löffler, 1993; Laux *et al.*, 1993; Ito, 1993, Chuah *et al.* 1999, 2001) All have shown that the reverse pulse pressure is usually not uniformly distributed along the filter element. It is generally agreed that pressure is highest at the close end of the candle and lowest, or even close to zero, at the open end.

Differential pressure measurements along the filter candles have been mostly performed at room temperature (Ito, 1993, Stephen *et al.*, 1996, Mai *et al.*, 1995, 1996). Measurements at high temperatures have been described and reported by Berbner and Löffler (1993), Hajek and Peukert (1995) and Ito *et al.* (1998). Table 1-1 summarises

* To whom the correspondence may be addressed.

the literature concerning the flow characteristics during cleaning of various ceramic filter candles.

Velocity measurements in ceramic filter elements during pulse cleaning have been carried out by Baik *et al.* (1993), Christ and Renz (1996), and Biffin *et al.* (1997). Baik *et al.* (1993) found that a new filter candle will exhibit a certain degree of inhomogeneity and has the possibility of blinding (dust cake remaining accumulated on the filter surface). This dust will remain on the candle surface after cleaning. These factors will severely affect the flow within the candle, both under operation and cleaning. Christ and Renz (1996) measured the axial velocity with a laser doppler Anemometer in order to validate the numerical simulations of a single filter element during pulse cleaning. Biffin *et al.* (1997) measured the axial velocity along the filter candle using a hot-wire probe. In their studies, a larger duration pulse showed no significant influence on the maximum velocity level inside the filter.

In this paper, a new simulation method for

Table 1-1. Overview of publication concerning flow characteristics during recleaning of various candle types

Candle Type (Manufacturer)	Properties					
	D_i mm	D_o mm	Length mm	Porosity, ε %	Resistance, kPa/(m/s)	Reference
Ceramic filter (not indicated)	40	60	500	30-48	n.i.	Kanaoka *et al.* (1999)
Tube filter (not indicated)	40	70	4000	n.i.	59.6	Ito (1993)
Tube filter (NGK)	40	70	1000	n.i.	n.i.	Ito *et al.* (1998)
Cerafil S-1000 (FOSECO)	40	60	1000	86	n.i.	Stephen *et al.* (1996)
KE85/150 (BWF)	110	150	1400	93	2	Berbner and Löffler (1993)
KE85/60 (BWF)	42	60	975	93	1	Hajek and Peukert (1995)
KE85/60 (BWF)	42	60	975	93	1	Mai *et al.* (1995, 1996)
Schumalith 40 (SUT)	30	60	1000	37	8.6	Mai *et al.* (1996)
Schumalith 20 (SUT)	40	60	1000	36	19.4	Mai *et al.* (1996)
DIA-Schumalith 10-20 (SUT)	40	60	1000	37	29.6	Mai *et al.* (1996)

n.i. : not indicated

predicting the flow field during filter cleaning process is proposed. A computer program has been written to model the flow of the reverse pulse air- from the cleaning bar nozzle to the dirty side of the filter. The program uses an iterative calculation mode and allows variables such as pulse pressure and filter geometry to be changed. The results are compared with the experimental data. The program was also used to predict the cleaning behaviour of a tapered filter element. In this geometry, diameter decreases from the open end to the close end.

This developed mathematical model provided a simple, quick and acceptable prediction of the pressure distribution in the filters. The model was able to predict the pressure drop and the velocity profile along a filter element during reverse flow cleaning. The information is useful in filter design and assist in understanding of cleaning mechanism.

Description of the Model

The simulation program includes calculation of the contributions of the nozzle jet and the entrained flow at the filter inlet. It then computes gas volume flow rate through the orifice and along the filter element. The details of the analysis of free jets are illustrated in Appendix 1.

Figure 1 shows the flow maldistribution in a filter during filtration operation. Airflow from the

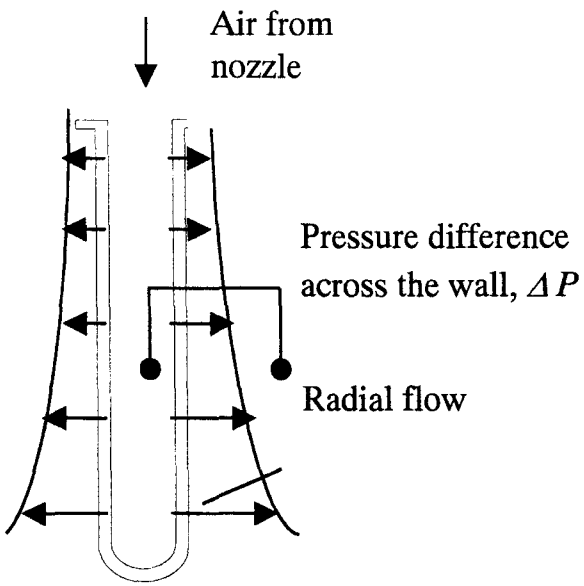

Figure 1: Flow maldistribution along filter during reverse pulse

cleaning bar is determined by reservoir pressure and hole diameter. The jet entrains more gas as it fans out towards the top of the filter element. At the top of the element, the gas mixture has an axial velocity which is determined by the airflow from the cleaning bar and the distance between the cleaning bar and the filter element.

At the bottom of the filter element, the axial velocity is zero. The internal pressure at this point is equal to the velocity at the top of the element minus friction loss between the two points. This internal pressure causes gas to flow radially through the filter wall. Gas flow rate is determined by the permeability of the filter medium and the internal pressure. The pressure drop across the wall is related to the resistance to flow of the filter medium and can be calculated using Darcy's Law for flow through a porous medium (in the appropriate form for a thick wall cylinder):

$$\Delta P = K\mu U\left[\ln\left(\frac{D_o}{Di}\right)\left(\frac{D_o}{2}\right)\right] \qquad (1)$$

Where K is resistance of the filter medium, m is the gas viscosity, D_o and D_i indicate the external and internal diameters of filter.

Above the bottom of the filter, the axial velocity is greater than zero and internal pressure is slightly less than at the bottom. The internal pressure generates further radial flow, resulting in greater axial flow and a decrease in internal pressure at the next position heading to the top of element.

Total radial flow is determined by inlet velocity and medium permeability. Total radial flow cannot exceed gas inlet flow. The mathematical description of this model is shown in the Appendix 2.

A computer program was developed to model the flow of the reverse pulse air from the cleaning bar nozzle to the dirty side of the filter. The program uses an iterative calculation mode of Microsoft Excel and allows variables such as reverse pulse pressure and filter geometry to be changed. Flow chart of the program is shown in Appendix 3.

General Experimental Method

Holes were drilled along the candle where a pitot tube was inserted as shown in Figure 2. Holes that were not in use were plugged. Air from the blower was injected into the open end of the

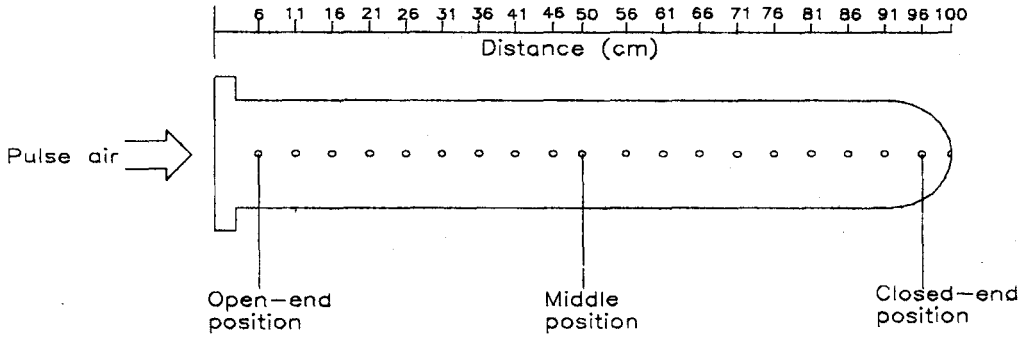

Figure 2: Candle measurement positions

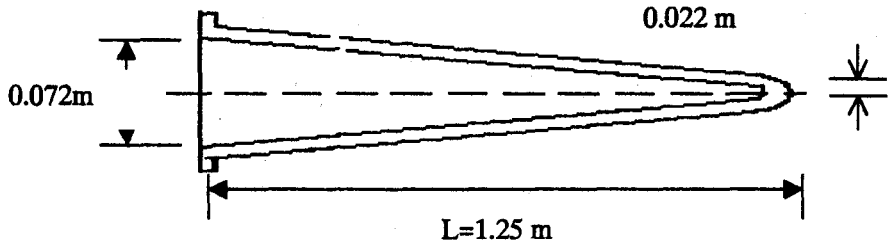

Figure 3: Schematic diagram of a tapered filter element

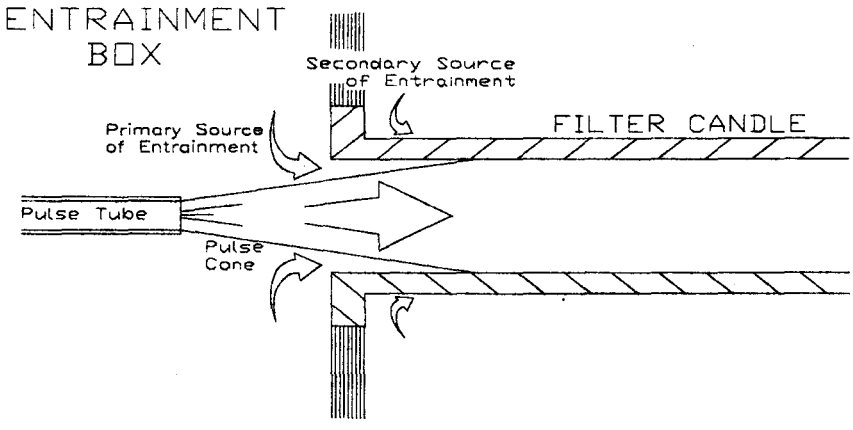

Figure 4: Pulse tube distance too short

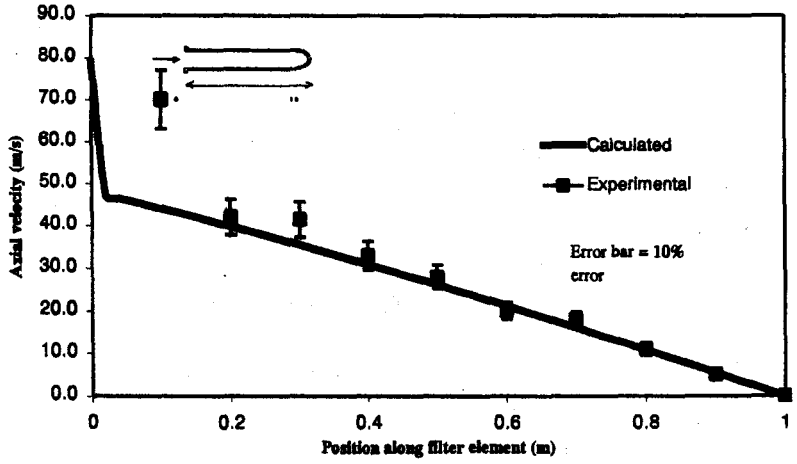

Figure 5: Profile of axial velocity for cylindrical filter, V=0.06m³/s

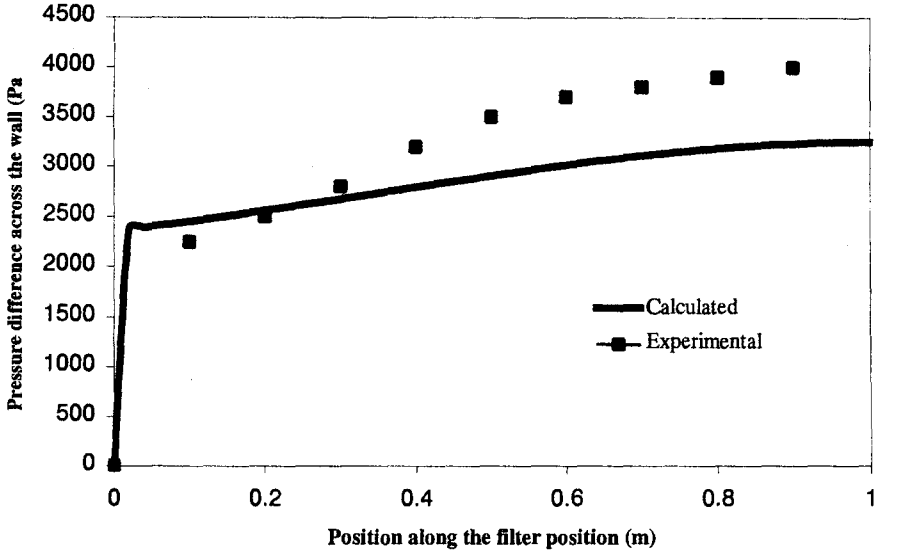

Figure 6: Pressure distribution for cylindrical filter, V= 0.06 m³/s

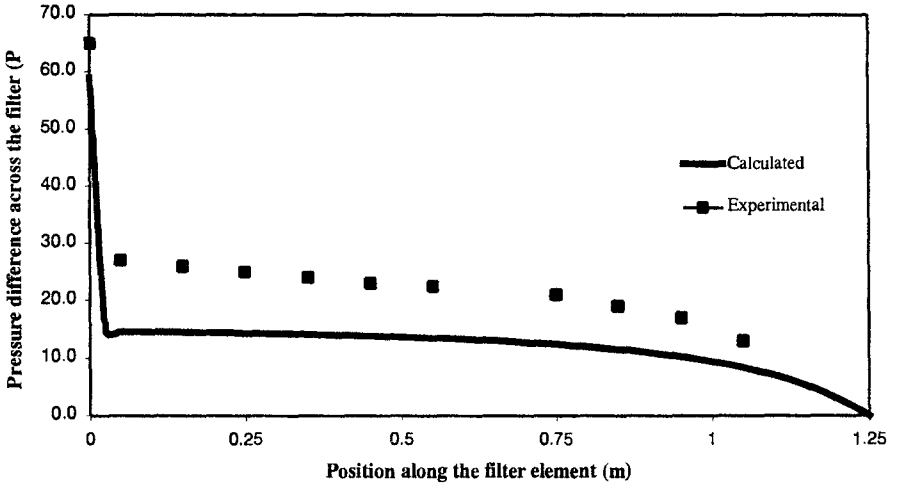

Figure 7:Profiles of axial velocity of tapered filter with a reverse flow

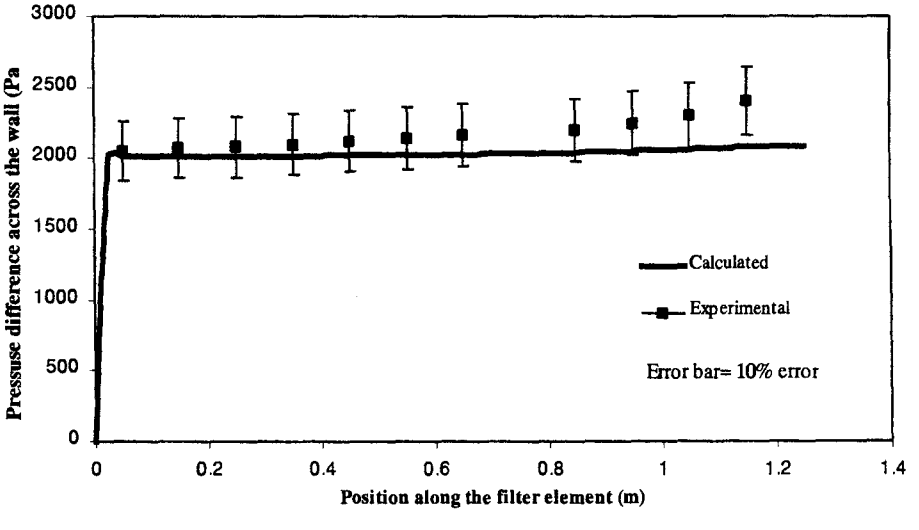

Figure 8: Pressure distribution for tapered filter with a reverse flow

filter candle. Pressure differences were measured by micromanometer.

A tapered filter geometry is shown in Figure 3.

Results and Discussion

Figures 5 and 6 show pressure distribution for a cylindrical filter candle with an entrance volumetric flow rate of 0.06 m^3/s. The simulation exhibited fair agreement with the experimental data for pressure distribution profile. Better agreement was found between simulation and experimental results for axial velocity.

The disagreement between the model and the experimental data at the distance close to the open end of the filter is caused by the secondary entrainment flow. Secondary entrainment is normally the result of the pulse tube being too close to the filter opening. As the gas was pulsed from the tube a large quantity of pulse gas extends into the filter. Secondary entrainment gas enters from the throat of the filter (Figure 4) in the opposite direction to the cleaning flow and will suck dusty gas through the round of throat of the filter. The model does not model the secondary entrainment and it is significant that the calculated results are different from the measured data at the open end of the filter.

The simulation of the tapered filter candle with an entrance reverse pulse pressure of 3 bar exhibited good agreement with the experimental results on both pressure distribution and axial velocity profiles. A more uniform pressure generation is found in the tapered filter than in the cylindrical filter.

CONCLUSION

The results showed that the mathematical model is able to predict the pressure drop and the velocity profile along a filter element for reverse flow cleaning. Both modelling and experimental results suggest that a more uniform pressure distribution is found in tapered elements. Simulations showed that the distance of the pulse tube has an effect on cleaning pressure distribution. A long pulse tube distance will increase the pressure difference in the filter due to larger volumetric gas flow converted into gas momentum which contributes to pressure differences across the filter wall. At longer distances, increment in pressure differences became less significant.

REFERENCES

Baik, S. M., Cheung, C. M. and Biffin, M., Velocity Measurements in Ceramic Candle Filter Elements, First International Environmental Engineering Conference, 1993, Leicester, UK.

Berbner, S., Löffler, F., "Pulse Cleaning of Rigid Ceramic Filter Elements at High Temperatures" in "Gas Cleaning at High Temperature" R.Clift and J.P.K. Seville (Eds.), Blackie Academic & Professional, Glasgow, 1993, pp. 225-243.

Biffin, M., Panagiotidis, P. and Pitsillides, C., "Velocity Measurements in a Ceramic Filter Element Undergoing Pulse Cleaning". Proceeding of the Institute of Mechanical Engineers, Part E: Journal of Process Mechanical Engineering, 1997, vol. 211, E1, pp.11-16.

Christ, A. and Renz, U, "Numerical Simulation of Single Ceramic Filter Element Cleaning" in "High Temperature Gas Cleaning", Schmidt, E., Gäng, Pitt, Ditter (Eds.), Institut für MUM, Universität Karlsruhe(TH), Karlsruhe, 1996, pp.728-739.

Chuah, T. G., Withers, C. J., Burbidge, A. S., Seville, J. P. K., "Numerical Modelling of Reverse Pulse Cleaning" in "High Temperature Gas Cleaning", A. Dittler, G. Hemmer, G. Kasper (Eds.), Institut für Mechanische Verfahrenstechnik und Mechanik der Universität Karlsruhe (TH), Karlsruhe, Glasgow, 1999, pp. 185-199.

Chuah, T. G., Withers, C. J., Burbidge, A. S., Seville, J. P. K., Numerical Modelling of Reverse Pulse Cleaning on Ceramic Filters, Symposium of Chemical Engineering Malaysia, 2001, Johor Bahru, Malaysia.

Hajek, St., Peukert, W., Experience with High Temperature Filter Media, PARTEC 95, Nürnberg, 1995, pp. 75-86.

Ito, S., "Pulse Jet Cleaning and Internal Flow in a Large Ceramic Tube Filter", in "Gas Cleaning at High Temperatures", R.Clift and J.P.K. Seville (Eds.), Blackie Academic & Professional, Glasgow, 1993, pp. 266-279.

Ito, S., Tanaka, T. and Kawamura, S., Changes in Pressure Loss and Face Velocity of Ceramic Candle Filters Caused by Reverse Cleaning in Hot Coal Gas Filtration, Powder Technology, 1998, vol. 100, pp. 32-40.

Kanaoka, C., Amornkitbamrung, M and Kishima, T., "Cleaning Mechanism of Dust from Ceramic Filter Element" in "High Temperature Gas Cleaning", A. Dittler, A., Hemmer, G., Kasper, G. (Eds.), Institut für Mechanische Verfahrenstechnik und Mechanik der Universität Karlsruhe(TH), Karlsruhe, 1999, pp.142-152.

Laux, S., Giernoth, B., Bulak, H., Renz, U., "Aspects of Pulse-Jet Cleaning of Ceramic Filter Elements" in "Gas Cleaning at High Temperatures" R.Clift and J.P.K. Seville (Eds.), Blackie Academic & Professional, Glasgow, 1993, pp.203-224.

Mai, R., Fronhöfer, M. and Leibold, H., Recleaning of Filter Candles by Fast Pressure Decrease on the Raw Gas Side, PARTEC 95, Nürnberg, 1995, pp. 301-310.

Mai, R., Fronhöfer, M. and Leibold, H., "Flow Charcteristics of Filter Candles During Recleaning" in "High Temperature Gas Cleaning", Schmidt, Gäng, Pitt, Ditter (Eds.), Institut für MUM, Universität Karlsruhe(TH), Karlsruhe, Germany, 1996, pp. 194-206.

Perry, R.H., Green, D. W., 1984 "Perry's Chemical Engineers' Handbook", 6th edition McGraw Hill., New York, p. 5-22

Rothwell E., Pulse-Driven Injectors for Fabric Dust Filters: (Part 1) The Significance of Jet-Injector Interaction, Filtration & Separation, September/October 1991, pp. 341-350.

Stephen, C.M., Grannell, S.K., Seville, J. P. K., "Conditioning and Pulse-Cleaning of Rigid Ceramic Filters", in "High Temperature Gas Cleaning", E. Schmidt, *et al.* (Eds), Institut für Mechanische Verfahrenstechnik und Mechhanik der Universität Karlsruhe (TH), Karlsruhe, 1996, pp. 207-218.

APPENDIX 1

A1.1 Analysis of free jets

A brief introduction to turbulent free jets is given by Perry and Green (1984) but a more detailed review is presented by Rothwell (1991) who studied the performance of venturi "injectors" as he refers to them and the nature of the pressure pulse generated.

A free jet, upon leaving an outlet, will entrain the surrounding fluid and expand as shown in Figure A1-1. The momentum of the fluid in the jet is transferred to the surrounding fluid being entrained. There is some loss in momentum due to turbulence and static-pressure gradients across the jet. A jet is considered to be free when its cross-sectional area is less than one fifth of the total cross-

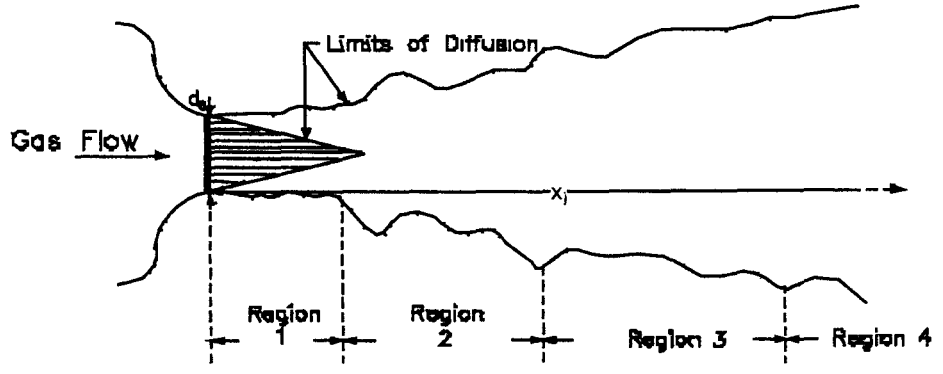

Figure A1-1: Configuration of a Turbulent Free Jet (after Perry and Green, 1984)

sectional flow area of the region through which it is flowing. A turbulent jet is considered to be a free jet whose jet Reynolds number is greater than 2000.

A1.1.1 Turbulent free-jet characteristics

There are four macroscopic regions in the development of the jet. The fist is the *flow establishment region* which occurs in the region $0<x_j<6.4d_n$ where the jet expands outwardly, entraining air from the surroundings (assumed stationary). The velocity of the central core is approximately equal to the initial jet velocity, $\bar{V}_{x_n}$.

The second region is the *transition region* between $6.4d_n<x_j<8d_n$ and in this region, the central core is eliminated. The next region lies in the range $8d_n<x_j<100d_n$ and is termed the *region of established flow* where expansion and entrainment continue. Finally the jet enters the *terminal region* at $x_j>100d_n$ where the centreline velocity decreases to zero.

Rothwell (1991) describes two rules of thumb to define the *jet angle* and the *outer limit of the jet.* The former is defined as the half-angle of the cone defined by the locus of the stream having half the centreline velocity. The latter is less well defined and is reported to vary with the initial state of the secondary air.

A1.1.2 Longitudinal distribution of velocity along the jet centre line

Rothwell and others have provided equations for the velocity variations within a jet. Consider a rounded-inlet circular jet where both jet fluid and entrained fluid are air:

$$\frac{\bar{V}_{x_jc}}{\bar{V}_{x_n}} = \frac{6.4\,d_n}{x_j} \quad for\ 7 < \frac{x_j}{d_n} < 100 \qquad \text{(A1-1)}$$

where the jet velocity along the centre line at the nozzle $\bar{V}_{x_n}$ = 10 to 50 m s^{-1}, $\bar{V}_{x_jc}$ is the velocity at distance x_j, d_n is the nozzle diameter and x_j is the distance along the jet centreline from the nozzle.

An expression is also provided for estimation of the velocity at a radial distance, y_j from the centerline:

A1.1.3 Radial distribution of longitudinal velocity

$$\log\left(\frac{\bar{V}_{x_jc}}{\bar{V}_{x_n}}\right) = 40\left(\frac{y_j}{x_j}\right)^2 \quad for\ 7 < \frac{x_j}{d_n} < 100 \qquad \text{(A1-2)}$$

A1.1.4 Jet angle

$$\alpha_j \approx 20° \quad \text{for } \frac{x_j}{d_n} < 100 \qquad \text{(A1-3)}$$

APPENDIX 2

a) Nozzle position and discharge rate

The optimum distance between the gas discharge orifice and the filter inlet, and the resulting gas flow rate through the orifice, are calculated based on basic fluid mechanics.

i) Distance from the nozzle to the filter element at optimum jet angle and perfect positioning (see Figure A2-1):

$$x = \frac{D_{or}}{2}\tan[((\alpha/2)/(360/2\pi))]^{-1} \qquad \text{(A2-1)}$$

ii) Gas volumetric flow rate for sonic flow through orifice of cross-section area, A_o:

$$q = \frac{C_1 C A_{or} \rho_g}{\sqrt{T_g}} = \pi \frac{D_{or}^2 C_1 C \rho_g}{4\sqrt{T_g}} \qquad \text{(A2-1)}$$

where C, C_1 are dimensionless constants and T_g is the absolute temperature of the gas stream.

b) Filter inlet

The entrance flow rate and the gas velocity entering the element are calculated.

iii) Total gas flow Q_{total} at the entrance of the filter element:

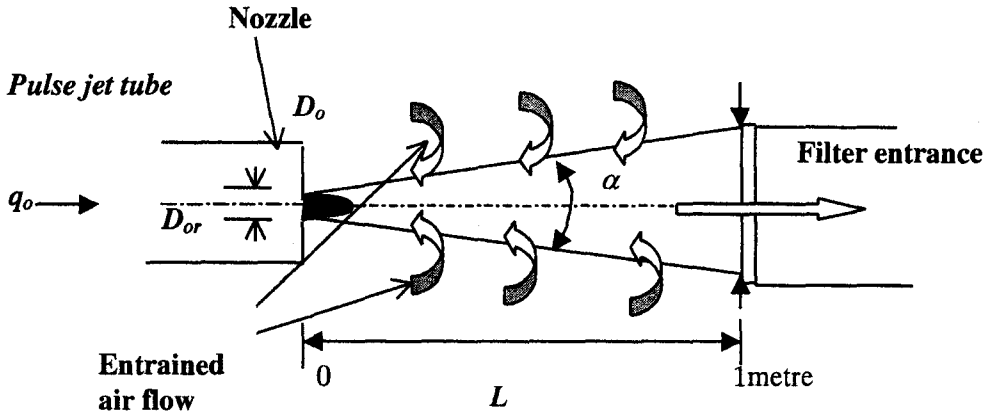

Figure A2-1: Schematic diagram of pulse gas flow for pulse jet tube and filter element

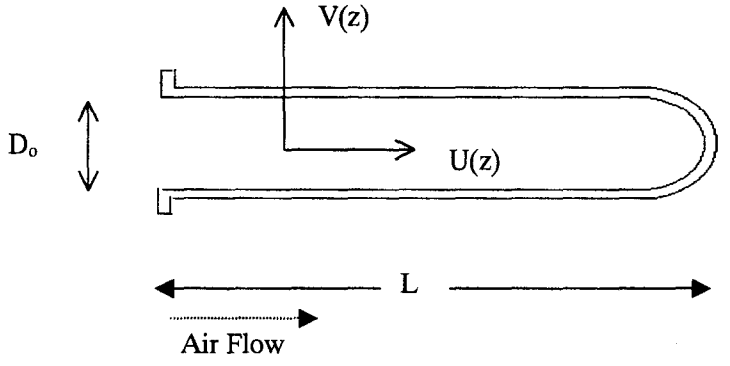

Figure A2-2: Schematic diagram of axial and radial directions flows in a filter of internal diameter, D_o, length, L and external pressure, P_o

$$Q_{total} = q_o(0.32)\frac{x}{D_o} \text{ for } 7 < \frac{x}{D_o} < 100 \quad \text{(A2-3)}$$

where x is the distance from the nozzle to the filter entrance.

iv) Velocity at the entrance of the filter element:

$$U = \frac{Q}{A_f} \quad \text{(A2-4)}$$

where A_f is the cross-sectional area at entrance of the filter.

v) Velocity head, static head equivalent of the kinetic energy in the stream of uniform velocity U_f (from Bernoulli's equation):

$$P_h = \frac{1}{2}U_f^2 \rho_g \quad \text{(A2-5)}$$

c) Filter tube

The length of the filter L is divided into equally spaced nodes, N. Starting from Eq. (*A2-6*) to Eq. (*A2-12*), pressure distribution is estimated by

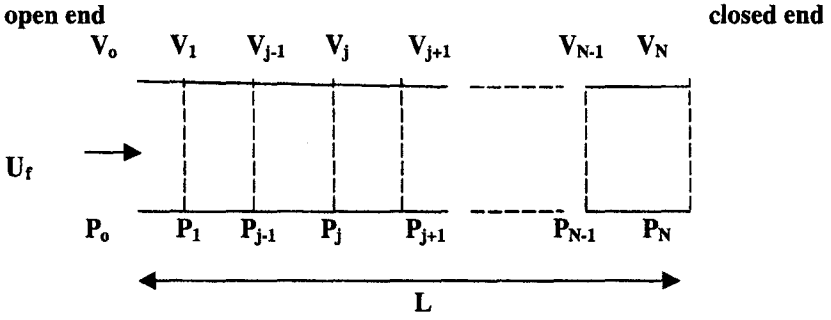

Figure A2-3: Description of flow in the filter element

iterative calculations of the parameters V_R, U_N and P along the filter element, taking into account element geometry and resistance. Boundary conditions, are (a) filtration pressure is provided at the inlet of the filter and (b) at the end of the filter, the volume flow rate is set to zero, *i.e.* no gas flow is permitted through the close end.

vi) Axial gas flow area, A_l:

$$A_{l,j} = \pi \frac{D_j^2}{4} \qquad \text{(A2-6)}$$

where D_j denotes the internal diameter of the filter at the position of the j-th node.

vii) Cylindrical surface area of radial gas flow at j-th node, A_R:

$$A_{R,j} = \pi D_j \frac{L}{N-1} \qquad \text{(A2-7)}$$

viii)Gas differential volume flow rate through filter element wall, V:

$$V_j = \left[\frac{A_{R,j}\Delta P_j}{K}\right] \qquad \text{(A2-8)}$$

where subscript j denotes the variables are evaluated at node-j.

ix) Cumulative loss of gas flow rate through the filter element walls preceding node-j:

$$F_j = \sum_1^j V_j \qquad \text{(A2-9)}$$

since there is no flux through the end of the filter at z=L, $Q = \sum_1^N V_j$

x) Axial superficial gas velocity at j-th position

$$U_j = U - \frac{F_j}{A_{l,j}} \qquad \text{(A2-10)}$$

xi) Static equivalent velocity head at j-th position:

$$P_{h,j} = U_j^2 \rho \qquad \text{(A2-11)}$$

xii) Static equivalent pressure head at j-th position

$$Pj = Phj \qquad \text{(A2-12)}$$

APPENDIX 3

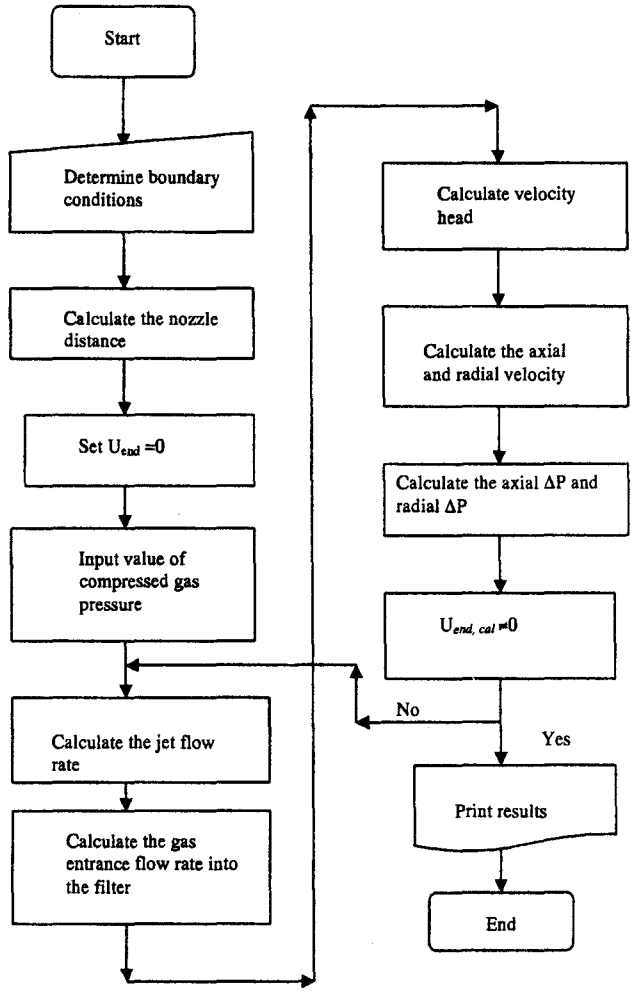

Figure A-3 Flow chart of the model